

Harmonic field in knotted space

Xiuqing Duan and Zhenwei Yao*

School of Physics and Astronomy, and Institute of Natural Sciences, Shanghai Jiao Tong University, Shanghai 200240, China



(Received 8 March 2018; published 25 April 2018)

Knotted fields enrich a variety of physical phenomena, ranging from fluid flows, electromagnetic fields, to textures of ordered media. Maxwell's electrostatic equations, whose vacuum solution is mathematically known as a harmonic field, provide an ideal setting to explore the role of domain topology in determining physical fields in confined space. In this work, we show the uniqueness of a harmonic field in knotted tubes, and reduce the construction of a harmonic field to a Neumann boundary value problem. By analyzing the harmonic field in typical knotted tubes, we identify the torsion driven transition from bipolar to vortex patterns. We also analogously extend our discussion to the organization of liquid crystal textures in knotted tubes. These results further our understanding about the general role of topology in shaping a physical field in confined space, and may find applications in the control of physical fields by manipulation of surface topology.

DOI: [10.1103/PhysRevE.97.040702](https://doi.org/10.1103/PhysRevE.97.040702)

Understanding physical fields in confined space is a common theme in a host of scientific problems, ranging from the classical examples in hydrodynamics [1–3] and electro-dynamics [4], to the fabrication of geometrically confined liquid crystals for various applications [5–8]. The topology of the domain can critically determine the configuration of a physical field [9,10]. Of special interest is the structure of a physical field filling knotted tubes. Knotted field configurations, previously known in Lord Kelvin's theoretical proposal of the vertex atom hypothesis inspired by the work of Helmholtz [11], have been experimentally accessible in diverse physical and chemical systems [12], including vortex loops in superconductors [13,14], defect loops in liquid crystals [15–22], toroidal nematic textures [8,23–26], and knotted beams of light [27–29]. Note that in these systems knotted fields mostly occur either in vacuum space or in the free space of viscous fluids and nematic liquid crystals. Past studies have shown that Maxwell's equations, despite their linearity, can admit topologically nontrivial knotted solutions in free space [27,29–35]. These results suggest that the system of Maxwell's equations provides an ideal setting to address the fundamental question of how topology shapes behaviors of physical fields in confined space.

The goal of this work is to construct vacuum solutions to Maxwell's electrostatic equations $\text{div } \mathbf{E} = \mathbf{0}$ and $\text{curl } \mathbf{E} = \mathbf{0}$ with tangential boundary condition in topologically nontrivial domains of knotted tubes. Such a solution is mathematically known as the harmonic field [10]. The existence of a nontrivial smooth harmonic field in confined space depends on the topology of the domain [10]. As an example, a smooth field is forbidden in spherical closed space; a singularity in the field is inevitable. However, toroidal space can admit a nontrivial vacuum solution [9].

In this work, we first show the uniqueness of the harmonic field as dictated by the topology of a knotted tube. By introducing an irrotational field, we reduce the construction

of the harmonic field to solving a Neumann boundary-value problem. The harmonic field in the circular tube (a standard torus) is analytically derived. For a torsion-free, elliptic torus with spatially varying curvature along its core loop, we find that the harmonic vector field becomes tilted, and its projection to the cross section of the tube exhibits a bipolar configuration. By further examining the projected harmonic field in the cross sections of trefoil and cinquefoil torus knots, we identify the torsion-driven transition from the bipolar to the vortex configurations. These results reflect the general feature of a knotted harmonic field that is beyond the specific Maxwell's equation system. As an example, we finally extend our discussion to the organization of nematic textures confined in knotted tubes.

Frenet-Serret parametrization of knotted tube. We construct the domain of a filled knotted tube from a closed loop γ ; it is named the core loop of the tube. A solid torus is a special case of a filled knotted tube. The arc-length parametrization of the loop γ is $\gamma : \mathbb{S}_L \rightarrow \mathbb{R}^3$, where $\mathbb{S}_L = [0, L]$, and L is the length of the loop. The domain inside the tube is denoted as $T_\epsilon(\gamma)$. $T_\epsilon(\gamma) = \{x \in \mathbb{R}^3 : \text{dist}(x, \gamma) < \epsilon\}$, where $\text{dist}(x, \gamma)$ is the distance between the point x and the loop γ , and ϵ is the thickness of the tube. ϵ is positive and sufficiently small to avoid self-intersect of the knotted tube.

To represent any point within the tube, we introduce the triple of $\{\gamma(\alpha), \mathbf{e}_1(\alpha), \mathbf{e}_2(\alpha)\}$ pointwise along the core loop, which are the tangent, normal, and binormal unit vectors, as shown in Fig. 1(a). These unit vectors form a moving frame of reference named the Frenet-Serret frame along the core loop [36,37]. The arc-length parameter $\alpha \in [0, L]$. The pair of the normal and binormal vectors define a two-dimensional unit disk denoted by D^2 [see Fig. 1(b)]. Any point in T_ϵ can therefore be represented by the coordinates $(\alpha, y_1, y_2) \in \mathbb{S}_L \times D^2$ via the diffeomorphism $(\alpha, y_1, y_2) \mapsto \gamma(\alpha) + \epsilon y_1 \mathbf{e}_1(\alpha) + \epsilon y_2 \mathbf{e}_2(\alpha)$. $y_1, y_2 \in [0, 1]$. The Euclidean metric in the tube is

$$ds^2 = A d\alpha^2 + 2\epsilon^2 \tau (y_2 dy_1 - y_1 dy_2) d\alpha + \epsilon^2 (dy_1^2 + dy_2^2),$$

where $A = (1 - \epsilon \kappa y_1)^2 + (\epsilon \tau)^2 (y_1^2 + y_2^2)$, and $\kappa \equiv \kappa(\alpha)$ and $\tau \equiv \tau(\alpha)$ are the curvature and torsion of the core

*zyao@sjtu.edu.cn

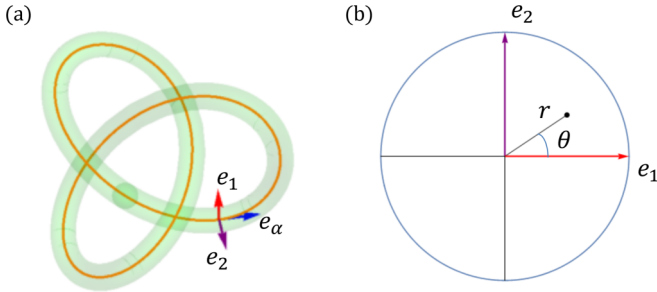


FIG. 1. Illustration of a knotted tube constructed out of the red core loop. (a) The tangent vector \mathbf{e}_α , normal vector \mathbf{e}_1 , and binormal vector \mathbf{e}_2 form a moving frame of reference named the Frenet-Serret frame along the core loop. (b) The pair of the normal and binormal vectors define a two-dimensional unit disk.

loop γ . The volume element $dV = \epsilon^2 B d\alpha dy_1 dy_2$, where $B = 1 - \epsilon\kappa y_1$.

Construction of harmonic field. All the harmonic fields, denoted as \mathbf{h} in the filled knotted tube T_ϵ , constitute a vector space [10]: $\mathcal{H}(T_\epsilon) = \{\mathbf{h} \in C^\infty(T_\epsilon, \mathbb{R}^3) : \text{div } \mathbf{h} = 0, \text{curl } \mathbf{h} = 0 \text{ and } \mathbf{h} \cdot \mathbf{v} = 0\}$, where $C^\infty(T_\epsilon, \mathbb{R}^3)$ denotes an infinitely differentiable functional space defined in T_ϵ , and \mathbf{v} is the unit outward normal vector on the surface of T_ϵ .

We first show the uniqueness of the harmonic field (up to a multiplicative constant) as a fundamental consequence of the topological structure of the space T_ϵ . The space $\mathcal{H}(T_\epsilon)$ is isomorphic to the first cohomology group $H^1(T_\epsilon)$ of the filled knotted tube T_ϵ , which is associated with the only noncontractible loop along the curve γ [10,36]. Furthermore, $H^1(T_\epsilon) \cong H^1(S^1 \times D^2) \cong H^1(S^1) \cong \mathbb{Z}$, where S^1 is a topological circle and D^2 is a topological disk [36]. Therefore, the space $\mathcal{H}(T_\epsilon)$ is one-dimensional in the sense that if \mathbf{h} is a harmonic vector field, then all the other harmonic vector fields are linear with \mathbf{h} [10,36]. Here, we emphasize that the topology of the filled knotted tube T_ϵ determines the existence and uniqueness of the harmonic field, which lays the foundation for the following construction of the harmonic field.

To construct the harmonic field in T_ϵ , we consider the vector field $\mathbf{h}_0 = B^{-2}(\partial_\alpha + \tau\partial_\theta)$, where $B = 1 - \epsilon\kappa y_1$, and θ is the polar angle as shown in Fig. 1(b). One can show that \mathbf{h}_0 is irrotational and satisfies the tangential boundary condition (the proof is given in Appendix A). Based on \mathbf{h}_0 , we construct a harmonic vector field by the Hodge decomposition [10,36]:

$$\mathbf{h} = \mathbf{h}_0 + \nabla\psi. \quad (1)$$

The divergence-free condition requires that the scalar function ψ in Eq. (1) must satisfy

$$\Delta\psi = \varrho \quad (2)$$

in T_ϵ with the boundary condition $\partial_\nu\psi|_{\partial T_\epsilon} = 0$. $\varrho = -\text{div } \mathbf{h}_0 = \epsilon B^{-3}r(\tau\kappa \sin\theta - \kappa'\cos\theta)$, satisfying $\int \varrho dV = 0$. The solution ψ is unique up to a constant. Therefore, the search for the harmonic vector field in T_ϵ is nicely reduced to the Neumann boundary value problem in Eq. (2).

The harmonic vector field can be derived analytically when the core loop γ is a circle, i.e., the tube is a standard solid torus. Since $\tau = 0$ and κ is a constant, the source term ϱ in Eq. (2)

vanishes. Multiplying Eq. (2) by ψ , we have

$$\begin{aligned} \int_{T_\epsilon} \psi \Delta\psi dV &= \int_{\partial T_\epsilon} \psi \partial_\nu\psi dS - \int_{T_\epsilon} |\nabla\psi|^2 dV \\ &= - \int_{T_\epsilon} |\nabla\psi|^2 dV = 0. \end{aligned}$$

Requiring $\nabla\psi = 0$ leads to the expression for the harmonic field:

$$\mathbf{h} = B^{-1}\mathbf{e}_\alpha = \frac{1}{1 - \epsilon\kappa y_1}\mathbf{e}_\alpha, \quad (3)$$

where \mathbf{e}_α is the unit tangent vector to the core loop γ (see Fig. 1). We recognize that Eq. (3) has the same functional form as that of the magnetic field generated by electric current in a straight wire.

For an elliptic core loop with spatially varying curvature $\kappa(\alpha)$, we numerically solve Eq. (2), and find that the harmonic vector field becomes tilted with a nonzero transverse component \mathbf{h}_\perp lying over the cross section of the tube, as shown in Fig. 2(b). In contrast, $\mathbf{h}_\perp = 0$ for the case of a standard solid torus. The triple numbers in the curly brackets in Fig. 2 are the values for t , the curvature $\kappa(t)$, and the torsion $\tau(t)$, respectively. t is a parametrization of the core loop. $t \in [0, 2\pi)$, corresponding to $\alpha \in [0, L)$. From Fig. 2(b), we see that the tilted harmonic vector field \mathbf{h}_\perp exhibits a bipolar configuration, and the entire field configuration rotates along the core loop. The strength of the \mathbf{h}_\perp field approaching the diametric poles becomes vanishingly small, which is consistent with the tangential boundary condition.

To examine the effect of torsion on the field configuration, we further consider knotted tubes constructed out of core loops with torsion. In Figs. 2(c) and 2(e), we show the trefoil and cinquefoil torus knots with crossing number three and five, respectively [38]. Their names are from the three-leaf clover plant and the five-petaled flowers of plants in the genus *Potentilla*. The trefoil knot is the simplest example of a nontrivial knot. From Figs. 2(d) and 2(f), we see that the configuration of the \mathbf{h}_\perp field becomes azimuthal, which is distinct from that in Fig. 2(b) for the case of a torsion-free core loop.

We further notice that, at the location of small torsion on the core loop, as shown in the last plot of Fig. 2(d), the \mathbf{h}_\perp field is in an intermediate state between the bipolar and vortex configurations. All these observations substantiate the physical scenario of torsion-driven transition from the bipolar to the vortex configurations. In all the torsion-driven vortex structures in Figs. 2(d) and 2(f), the field strength near the center becomes zero to avoid singularity. It is of interest to note that the transformation of the \mathbf{h}_\perp field from the bipolar to the vortex structure resembles the merge of a pair of $+1/2$ defects into a single $+1$ defect in nematic textures over spherical disks [39].

Nematic texture in knotted tube. Now, we extend our discussion to the system of nematic liquid crystal (LC) confined in a knotted tube. Self-assembly of LC in various confined environments especially within the cylindrical polymer sheath represents a new trend in LC research for promising applications in the new generation of wearable technology devices [8]. The experimentally accessible system of a LC-filled knotted tube is an ideal model to address the inquiry into the

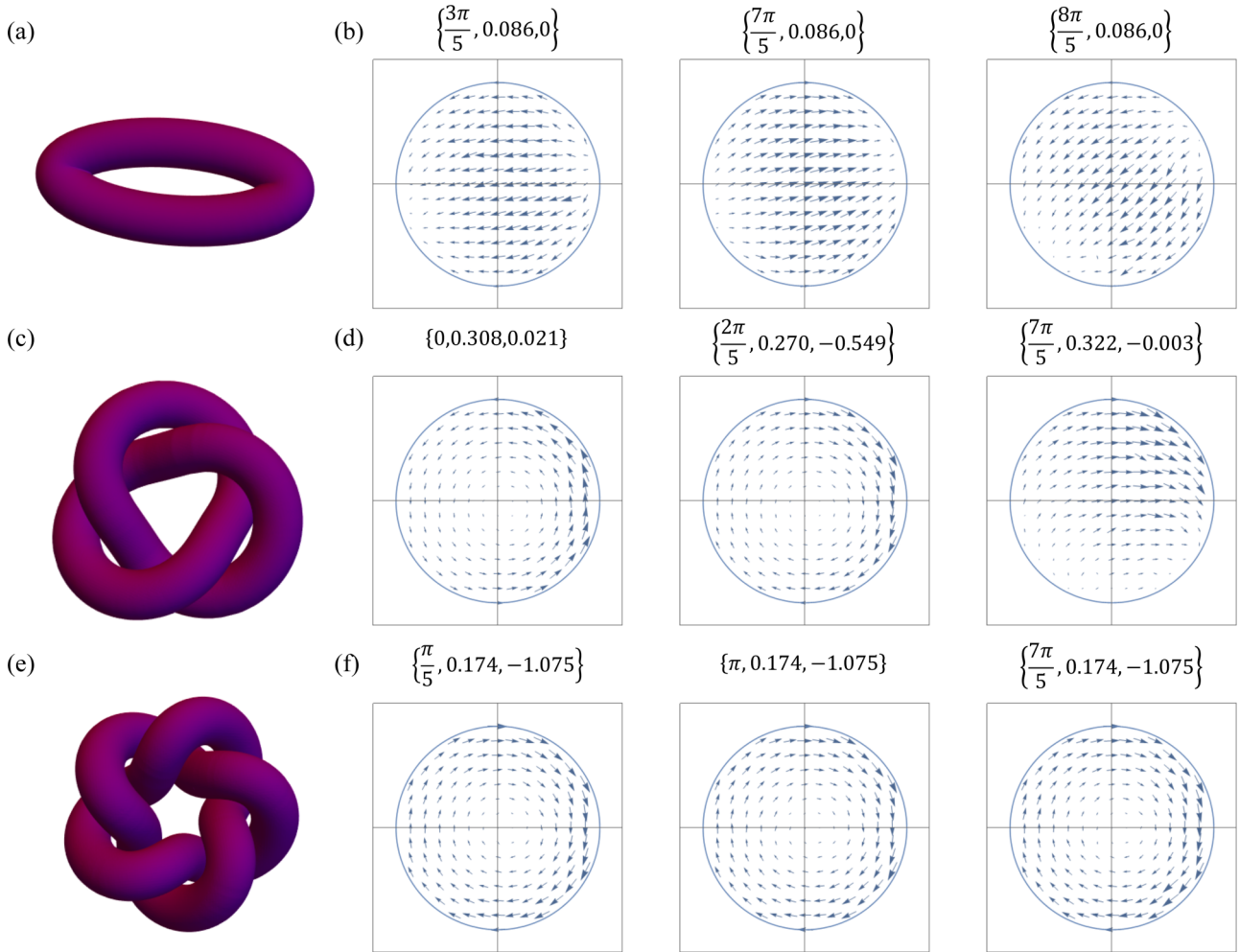


FIG. 2. Visualization of the harmonic field projected to the cross section of typical knotted tubes. (a), (b) Solid ellipse torus: $(4.6 \cos t, 1.6 \sin t, 0)$. (c), (d) Trefoil knot: $(10/9)\{[3 + \cos(3t)]\cos(2t), [3 + \cos(3t)]\sin(2t), \sin(3t)\}$. (e), (f) Cinquefoil torus knot: $\{[3 + 1.1\cos(5t)]\cos(2t), [3 + 1.1\cos(5t)]\sin(2t), 2\sin(5t)\}$. The triple numbers in the curly brackets are the values for t , the curvature $\kappa(t)$, and the torsion $\tau(t)$, respectively. $t \in [0, 2\pi)$. The thickness of all these knots is $\epsilon = 1$.

organization of matter by the topology of the domain. In the following, we discuss how our preceding discussions on harmonic field yield insights into this question. We consider a planar boundary condition where LC molecules at the boundary lie in the tangent plane [40].

In the continuum limit, the orientations of LC molecules are characterized by a director field $\mathbf{n}(x)$. \mathbf{n} is a unit vector and $\mathbf{n} \equiv -\mathbf{n}$ due to the apolar nature of LC molecules. According to the Frank free-energy model for nematics, the free-energy cost associated with the deformation of the director field from the uniform state is [40]

$$F[\mathbf{n}(\mathbf{x})] = \int f dV - K_{24} \int dS \cdot \mathbf{g}_{24}, \quad (4)$$

where $f = \frac{1}{2}K_1(\nabla \cdot \mathbf{n})^2 + \frac{1}{2}K_2(\mathbf{n} \cdot \nabla \times \mathbf{n})^2 + \frac{1}{2}K_3(\mathbf{n} \times \nabla \times \mathbf{n})^2$. K_1 , K_2 , and K_3 are the splay, twist, and bending moduli, respectively. In the surface term, K_{24} is the saddle-splay modulus, and $dS = \mathbf{v} dS$ is the area element, where \mathbf{v} is the outward unit normal vector on the surface. $\mathbf{g}_{24} = \mathbf{n}\nabla \cdot \mathbf{n} + \mathbf{n} \times \nabla \times \mathbf{n}$.

Both the volume and surface terms in the expression for the Frank free energy F in Eq. (4) vanish when \mathbf{n} is a harmonic field whose divergence and curl are zero. However, our preceding

discussion shows that the expression for the harmonic field takes the form of $\mathbf{h} = B^{-2}(\partial_\alpha + \tau \partial_\theta) + \nabla \psi$, and it is not a unit vector, which is in conflict with the condition of $|\mathbf{n}| = 1$. Consequently, in general, the Frank free energy of the ground-state nematic texture in a knotted tube must be nonzero, as dictated by the topology of the domain. It is of interest to study the minimization of the Frank free energy via the interplay of the director field and the geometry of the knotted tube. As an analytically tractable case, we work in the constraint of an untilted director field, and derive that a torsion-free tube tends to take a circular shape to minimize the free energy. The details are presented in Appendix B.

In summary, we study the problem of the harmonic field confined in knotted space that is inspired by solving for the vacuum solution to Maxwell's electrostatic equations. We show that the topology of a knotted tube determines the existence and uniqueness of the harmonic field, and reduce the construction of a harmonic field to a Neumann boundary value problem. From the solved harmonic field in typical knotted tubes, we identify the torsion-driven transition from bipolar to vortex patterns. We also analogously extend our discussion to the organization of liquid crystal textures in knotted tubes.

These results further our understanding about how topology shapes behaviors of physical fields in confined space, and may find applications in the control of physical fields by the manipulation of surface topology.

Acknowledgments. This work was supported by NSFC Grant No. 16Z103010253, the SJTU startup fund under Grant No. WF220441904, and the award of the Chinese Thousand Talents Program for Distinguished Young Scholars under Grants No. 16Z127060004 and No. 17Z127060032.

APPENDIX A: PROOF OF THE IRROTATIONAL NATURE OF \mathbf{h}_0

The coordinate-independent expression for the curl operator is $\text{curl} \mathbf{n} = (\star d n^\flat)^\sharp$, where \star is an operator called Hodge dual, and \flat and \sharp are the musical isomorphisms [36,37,41]. We calculate $\text{curl} \mathbf{h}_0$ step by step. $\mathbf{h}_0^\flat = AB^{-2}d\alpha + (-\epsilon^2\tau r^2)B^{-2}d\theta + (-\epsilon^2\tau r^2)B^{-2}\tau d\alpha + \epsilon^2r^2\tau B^{-2}d\theta = d\alpha$, where the last equality is by inserting A and B , whose expressions are given in the main text. So we have $dh_0^\flat = dd\alpha = 0$. Consequently, $\text{curl} \mathbf{h}_0 = (\star dh_0^\flat)^\sharp = 0$.

APPENDIX B: OPTIMAL GEOMETRY OF TORSION-FREE, NEMATICS-FILLED TUBE

In this section, we will show that a torsion-free tube filled with nematics tends to take a circular shape to minimize the Frank free energy. We first represent the director \mathbf{n} by $\mathbf{n} = n_1(\alpha, r, \theta)\mathbf{e}_\alpha + n_2(\alpha, r, \theta)\mathbf{e}_r + n_3(\alpha, r, \theta)\mathbf{e}_\theta$, where $\mathbf{e}_\alpha = \frac{1}{\sqrt{A}}\partial_\alpha$, $\mathbf{e}_r = \frac{1}{r}\partial_r$, and $\mathbf{e}_\theta = \frac{1}{r}\partial_\theta$ are unit basis vectors.

To make the minimization of Frank free energy analytically tractable, our discussion is limited to the torsion-free tube whose core loop is a planar curve. Furthermore, we work in the constraint that the radial component of the director field is zero and the nematic texture has axial symmetry [42]. That is, $n_2(\alpha, r, \theta) = 0$, and \mathbf{n} is independent of θ . Therefore, $\mathbf{n} = n_1(\alpha, r)\mathbf{e}_\alpha + n_3(\alpha, r)\mathbf{e}_\theta$. Since \mathbf{n} is a unit vector, the simplest case is $\mathbf{n} = \mathbf{e}_\alpha$, i.e., all the lines of the director are along the core loop of the tube.

Under these prescribed constraints, we derive for the following Euler-Lagrange equation:

$$\partial_k \frac{\partial f}{\partial \left(\frac{\partial n_i}{\partial x_k}\right)} + \frac{\partial_k \sqrt{g}}{\sqrt{g}} \frac{\partial f}{\partial \left(\frac{\partial n_i}{\partial x_k}\right)} - \frac{\partial f}{\partial n_i} = -\lambda n_i.$$

The condition of $n_3 = 0$ requires $\kappa'(\alpha)$ to be 0. In other words, the core loop of the elliptic tube must be a circle to satisfy the Euler-Lagrange equation. Such a circular torus solution turns out to be a minimum of the Frank free energy by the following numerical analysis.

Consider an elliptic core loop; after some calculation, we find that only the bending term in Eq. (4) is nonzero:

$$F = K_3\pi\epsilon^2 \int_0^{2\pi} \frac{\kappa(t)^2}{1 + \sqrt{1 - \epsilon^2\kappa(t)^2}} (\sqrt{a^2\sin^2 t + b^2\cos^2 t} dt), \quad (\text{B1})$$

where $\kappa = ab/(a^2\sin^2 t + b^2\cos^2 t)^{3/2}$. a and b are the semimajor and semiminor axes. Numerical analysis of Eq. (B1) shows that F monotonously decreases with b . Since $b \leq a$, the optimal shape is therefore a circular torus. By inserting $b = a$ in Eq. (B1), we have $F_{\min}/(K_3\pi\epsilon^2) = 2\pi/(a + \sqrt{a^2 - \epsilon^2})$.

-
- [1] D. Kleckner and W. T. Irvine, *Nat. Phys.* **9**, 253 (2013).
[2] M. W. Scheeler, D. Kleckner, D. Proment, G. L. Kindlmann, and W. T. Irvine, *Proc. Natl. Acad. Sci. USA* **111**, 15350 (2014).
[3] M. W. Scheeler, W. M. van Rees, H. Kedia, D. Kleckner, and W. T. Irvine, *Science* **357**, 487 (2017).
[4] H. Kedia, I. Bialynicki-Birula, D. Peralta-Salas, and W. T. M. Irvine, *Phys. Rev. Lett.* **111**, 150404 (2013).
[5] H. K. Bisoyi and S. Kumar, *Chem. Soc. Rev.* **40**, 306 (2011).
[6] G. P. Alexander, B. Gin-ge Chen, E. A. Matsumoto, and R. D. Kamien, *Rev. Mod. Phys.* **84**, 497 (2012).
[7] S. Umadevi, X. Feng, and T. Hegmann, *Adv. Funct. Mater.* **23**, 1393 (2013).
[8] M. Urbanski, C. G. Reyes, J. Noh, A. Sharma, Y. Geng, V. S. R. Jampani, and J. P. Lagerwall, *J. Phys.: Condens. Matter* **29**, 133003 (2017).
[9] J. Klauder and J. A. Wheeler, *Rev. Mod. Phys.* **29**, 516 (1957).
[10] A. Enciso and D. Peralta-Salas, *Acta Math.* **214**, 61 (2015).
[11] W. Thomson, *Philos. Mag. (1798-1977)* **34**, 15 (1867).
[12] K. E. Horner, M. A. Miller, J. W. Steed, and P. M. Sutcliffe, *Chem. Soc. Rev.* **45**, 6432 (2016).
[13] A. V. Samokhvalov, *Physica C (Amsterdam)* **259**, 337 (1996).
[14] Z. Tesanović, *Phys. Rev. B* **59**, 6449 (1999).
[15] I. I. Smalyukh, Y. Lansac, N. A. Clark, and R. P. Trivedi, *Nat. Mater.* **9**, 139 (2010).
[16] U. Tkalec, M. Ravnik, S. Čopar, S. Žumer, and I. Mušević, *Science* **333**, 62 (2011).
[17] S. Čopar, T. Porenta, and S. Žumer, *Phys. Rev. E* **84**, 051702 (2011).
[18] S. Čopar, T. Porenta, and S. Žumer, *Liq. Cryst.* **40**, 1759 (2013).
[19] A. Martínez, M. Ravnik, B. Lucero, R. Visvanathan, S. Žumer, and I. I. Smalyukh, *Nat. Mater.* **13**, 258 (2014).
[20] S. Čopar, *Phys. Rep.* **538**, 1 (2014).
[21] S. Čopar, U. Tkalec, I. Mušević, and S. Žumer, *Proc. Natl. Acad. Sci. USA* **112**, 1675 (2015).
[22] P. J. Ackerman and I. I. Smalyukh, *Phys. Rev. X* **7**, 011006 (2017).
[23] E. Páram, J. Vallamkondu, V. Koning, B. C. van Zuiden, P. W. Ellis, M. A. Bates, V. Vitelli, and A. Fernandez-Nieves, *Proc. Natl. Acad. Sci. USA* **110**, 9295 (2013).
[24] Bryan Gin-ge Chen, P. J. Ackerman, G. P. Alexander, R. D. Kamien, and I. I. Smalyukh, *Phys. Rev. Lett.* **110**, 237801 (2013).
[25] V. Koning, B. C. van Zuiden, R. D. Kamien, and V. Vitelli, *Soft Matter* **10**, 4192 (2014).
[26] P. J. Ackerman, J. Van De Lagemaat, and I. I. Smalyukh, *Nat. Commun.* **6**, 6012 (2015).
[27] W. T. Irvine and D. Bouwmeester, *Nat. Phys.* **4**, 716 (2008).
[28] M. R. Dennis, R. P. King, B. Jack, K. O'Holleran, and M. J. Padgett, *Nat. Phys.* **6**, 118 (2010).

- [29] W. T. Irvine, *J. Phys. A* **43**, 385203 (2010).
- [30] H. Bateman, *The Mathematical Analysis of Electrical and Optical Wave-Motion on the Basis of Maxwell's Equations* (University University Press, Cambridge, UK, 1915).
- [31] R. Penrose, *J. Math. Phys.* **8**, 345 (1967).
- [32] A. F. Rañada, *Lett. Math. Phys.* **18**, 97 (1989).
- [33] A. F. Ranada, *J. Phys. A* **25**, 1621 (1992).
- [34] C. Hoyos, N. Sircar, and J. Sonnenschein, *J. Phys. A* **48**, 255204 (2015).
- [35] H. Kedia, D. Foster, M. R. Dennis, and W. T. M. Irvine, *Phys. Rev. Lett.* **117**, 274501 (2016).
- [36] M. Nakahara, *Geometry, Topology, and Physics* (CRC Press, Boca Raton, FL, 2003).
- [37] M. Berger, *A Panoramic View of Riemannian Geometry* (Springer Science & Business Media, Berlin, 2012).
- [38] C. C. Adams, *The Knot Book: An Elementary Introduction to The Mathematical Theory of Knots* (American Mathematical Society, Providence, RI, 2004).
- [39] X. Duan and Z. Yao, *Phys. Rev. E* **95**, 062706 (2017).
- [40] M. Kleman and O. D. Laverntovich, *Soft Matter Physics: An Introduction* (Springer Science & Business Media, Berlin, 2007).
- [41] P. Mikusinski and M. Taylor, *An Introduction to Multivariable Analysis From Vector to Manifold* (Springer Science & Business Media, Berlin, 2012).
- [42] I. Kulić, D. Andrienko, and M. Deserno, *Europhys. Lett.* **67**, 418 (2004).